Geochemistry Geophysics Geosystems G3

Published by AGU and the Geochemical Society

Article
Volume 14, Number 4
5 April 2013
doi:10.1002/ggge.20048
ISSN: 1525-2027

Re-evaluating genetic models for porphyry Mo mineralization at Questa, New Mexico: Implications for ore deposition following silicic ignimbrite eruption

Joshua M. Rosera
Department of Geological Sciences, University of North Carolina, Chapel Hill, North Carolina, USA

Chevron Mining Inc., Questa, New Mexico, USA

Drew S. Coleman
Department of Geological Sciences, University of North Carolina, Chapel Hill, North Carolina, USA (dcoleman@unc.edu)

Holly J. Stein
AIRIE Program, Department of Geosciences, Colorado State University, Fort Collins, Colorado, USA

Physics of Geological Processes, University of Oslo, Oslo, Norway

[1] The Questa porphyry Mo deposit in New Mexico provides a unique opportunity to study the relationship between pluton assembly and mineralization in a long-lived volcanic field. Magmatism along the caldera margin initiated at ~25.20 Ma and continued for ~770 ka. During this time, the emplacement of mineralizing intrusions progressed westward and culminated in the assembly of the Questa Mo deposit between 24.76 Ma and 24.50 Ma. Molybdenite Re/Os geochronology shows that mineralization occurred in multiple pulses without thermal resetting of the chronometer. Because most of the molybdenite samples used in this study are from previous fluid inclusion studies, we treat Re/Os molybdenite as a new thermochronometer. Molybdenite Re/Os ages are integrated with zircon U/Pb ages to evaluate the cooling histories within the Mo deposit. This study suggests that individual cycles of magma emplacement and mineralization cooled rapidly. In contrast to prior genetic models for the Questa Mo deposit, these data show that the mineralizing intrusions were generated via rapid melt generation, separation, and intrusion into the shallow crust without involvement in a long-lived magma chamber. It is proposed that the anomalously high magma flux event associated with ignimbrite eruption transferred materials (Mo, volatiles) from the upper mantle necessary for immediately subsequent mineralization. Partial melting and scavenging within a deep-crustal hybridized zone generated Mo-rich magma that ascended to form the Questa deposit. Moreover, this hypothesis predicts an important connection between caldera-forming systems and porphyry-style mineralization that could be incorporated into future exploration models.

Components: 12,100 words, 8 figures, 2 tables.

Keywords: Molybdenum; Mineral occurrences and deposits; Hydrothermal systems; Radioisotope geochronology; Thermochronology; Pluton emplacement.

Index Terms: Mineral occurrences and deposits: Hydrothermal systems: Radioisotope geochronology: Thermochronology: Pluton emplacement.

Received 11 July 2012; **Revised** 16 November 2012; **Accepted** 16 December 2012; **Published** 5 April 2013.

Rosera, J. M., D. S. Coleman, and H. J. Stein (2013), Re-evaluating genetic models for porphyry Mo mineralization at Questa, New Mexico: Implications for ore deposition following silicic ignimbrite eruption, *Geochem. Geophys, Geosyst.*, *14*, 787–805, doi:10.1002/ggge.20048.

1. Introduction

[2] In 2010, the United States produced over $800 million of molybdenum oxide [*USGS MCS*, 2011], and the demand for Mo as an alloying agent in high-grade steel will likely increase as global economies recover. The majority of the world's Mo reserves are contained within porphyry Cu (± Mo) and porphyry Mo (± Cu) deposits. Although porphyry Mo deposits are often volumetrically smaller than porphyry Cu systems, they are still a significant source of Mo owing to higher ore grades.

[3] Understanding the timing of mineralization within a magmatic system is important for making accurate regional ore predictions. High-silica granite-related porphyry Mo deposits (Climax-type deposits) are often interpreted to form as cupolas above larger, more dynamic, magma chambers [*Wallace et al.*, 1968; *White et al.*, 1981; *Carten et al.*, 1988a, 1988b, 1993; *Lowenstern*, 1994; *Burnham*, 1997; *Klemm et al.*, 2008]. The depth and size of the magma body, as well as trends in chemical variation, remain topics of debate [*Keith et al.*, 1986; *Carten et al.*, 1993; *Audétat*, 2010]. Outstanding questions include: (1) How large is the magma chamber from which mineralizing cupolas originate? (2) At what depth in the crust do these magmas exist? (3) What is the mechanism for concentrating Mo?

[4] In a study of the chemistry, age, and tectonic setting of porphyry Mo deposits, *Carten et al.* [1993] observed that mineralization typically occurs late within the lifespan of long-lived (> 1 Ma) magmatic provinces. For example, at Questa, New Mexico (Figure 1), Mo mineralizing magmas intruded along the southern margin of the Questa caldera and

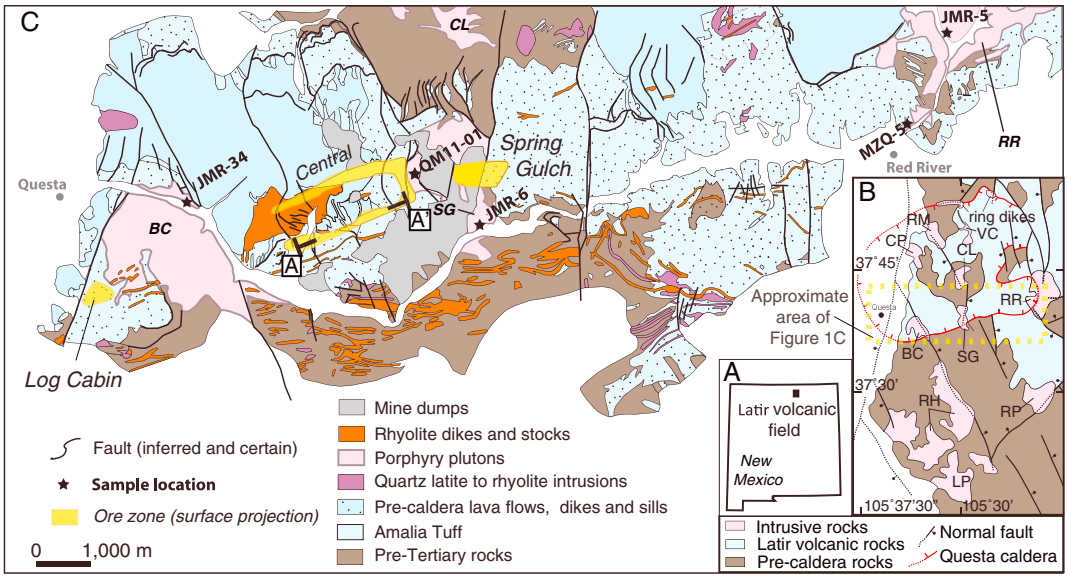

Figure 1. a) Map showing the location of the study area in New Mexico. b) Inset shows simplified geologic map of the Latir volcanic field, after *Lipman and Reed* [1989]. Pluton name abbreviations: CP, Cañada Pinabete; RM, Rito del Medio; VC, Virgin Canyon; CL, Cabresto Lake; BC, Bear Canyon; SG, Sulphur Gulch; RR, Red River; RH; Rio Hondo; RP, Relica Peak. c) Detailed map of the southern caldera margin showing U/Pb zircon sample locations. Ore zones approximately correspond to 0.2 wt.% MoS_2 contours projected to the surface. After *Meyer* [1991]. Pluton labels as in Figure 1b. Cross section A-A′ shown in Figure 2. Note that the caldera margin fault inferred from the work of *Lipman and Reed* [1989] approximately follows the Red River valley (gap in geology between the towns of Questa and Red River).

are interpreted to represent cupolas of an extensive late ring intrusion [*Lipman*, 1988]. Hydrothermal mineralization associated with ring faults is also observed in the Southern Rocky Mountain Volcanic Field in Colorado [*Lipman*, 2006] and at Round Mountain, Nevada [*Henry et al*., 1997] and the Borovista caldera in Bulgaria [*Singer and Marchev*, 2000].

[5] Climax-type deposits are thought to form during multiple magmatic-hydrothermal events that occur close in space and time [e.g., *Wallace et al*., 1968; *White et al*., 1981; *Carten et al*., 1988a]. Some models for Mo mineralization rely on simplified assumptions about the thermal history of plutons associated with the deposits. For example, *Burnham* [1997] modeled the formation of porphyry ore deposits above plutons intruded as large bodies of mostly liquid magma with simple cooling histories. More recently, *Seedorff and Einaudi* [2004a] analyzed overprinted alteration assemblages along cross-cutting veins to derive a pseudocyclical thermal evolutionary model for the Henderson porphyry Mo deposit in Colorado. These authors note that unidirectional models (simple high- to low-temperature through time, [*Lowell and Guilbert*, 1970; *Fournier*, 1999]) are of limited use for understanding the complexities observed within these deposits.

[6] The suggestion that thermal cycling is important to development of Climax-type Mo deposits is consistent with recent studies that indicate plutons are assembled episodically and have more complex thermal histories than that of a single intrusion [e.g., *Coleman et al*., 2004; *Seedorff and Einaudi*, 2004a, 2004b; *Davis et al*., 2012]. However, studying the relationship between porphyry-style mineralization and sub-adjacent magma reservoirs is largely inhibited by the lack of exposure of cogenetic rocks. The Questa porphyry Mo system presents an opportunity to study this relationship because intrusions of varying volume and emplacement depths are exposed throughout the Latir volcanic field. Additionally, because the system is relatively young, abundant pre-, syn-, and (some) post-caldera volcanic rocks [*Lipman et al*., 1986] are preserved.

[7] Detailed geo-thermochronology allows evaluation of the link between magmatism and Mo mineralization at Questa. Combining zircon U/Pb with more recently developed molybdenite Re/Os geochronology allows for full characterization of the temperature-time (T-t) history of the Questa deposit and places the mineralization into the magmatic and thermal history of the system. Applying this approach: (1) lends insight into the timing and duration of magma emplacement relative to Mo mineralization, (2) characterizes how porphyry Mo systems relate to the evolution of a long-lived volcanic field and shallow pluton assembly, and (3) evaluates the applicability of Re/Os molybdenite as a new thermochronometer.

2. Geological Setting

[8] The Questa porphyry Mo deposit is located in the New Mexico portion of the Southern Rocky mountain volcanic field. It is part of the Latir volcanic field (~ 1200 km^2) [Figure 1; *Lipman et al*., 1986]. Uplift and erosion along the eastern flank of the Rio Grande rift exposed a vertical section of volcanic strata and shallow plutons of the Latir field. Volcanism in the field began at 28.5 Ma with the eruption of dominantly andesite with local dacite and rhyolite [*Zimmerer and McIntosh*, 2012] and climaxed with the eruption of the ~500 km^3 Amalia Tuff at 25.52 ± 0.06 Ma [*Tappa et al*., 2011].

[9] Exposed plutonic rocks at Questa span ~6 Ma of intrusive history (~ 25.6–19.1 Ma; *Tappa et al*., 2011; *Zimmerer and McIntosh*, 2012) and become younger to the south. Caldera margin plutons are intermediate in age among exposed plutonic rocks and are associated with mineralization [*Meyer and Foland*, 1991; *Zimmerer and McIntosh*, 2012]. From east to west, the caldera margin plutons include the Red River intrusive complex, Sulphur Gulch pluton, Southwest intrusive suite, and the Bear Canyon pluton. The Red River intrusive complex (~ 24.96 Ma; *Zimmerer and McIntosh*, 2012) is a high-silica rhyolite to aplite porphyry dike complex that cuts granodiorite and fine-grained monzonite [*Lipman*, 1988]. Epithermal Au-Ag veins occur near the contact of the Red River intrusive complex [*McLemore and North*, 1984]. The Sulphur Gulch pluton includes granite porphyry (~ 24.73 Ma, *Zimmerer and McIntosh*, 2012) and biotite-plagioclase porphyry phases. Drilling and cross-sections developed at the Questa mine site indicate that the two phases of the Sulphur Gulch pluton are connected at depth [*SRK Consulting*, *Inc. report*]. Also at depth, the Sulphur Gulch pluton is in contact with the Southwest intrusive suite, which includes granite, aplite, rhyolite, and latite associated with, and locally hosting, Mo mineralization [*Ross et al*., 2002]. The Bear Canyon pluton (~ 24.37 Ma, *Zimmerer and McIntosh*, 2012) is similar to the granitic phase of the Sulphur Gulch pluton and grades from aplite to granite porphyry.

[10] The roofs of the mineralizing intrusions at Questa dip at a low angle to the north and likely

followed a pre-existing anisotropy [*Ross et al.*, 2002] that may be related to the low-angle normal faults observed throughout the southern caldera margin [*Meyer and Foland*, 1991]. These faults are believed to have originally formed at high angles and were subsequently rotated to low angles above a batholith underlying the southern caldera margin [*Meyer and Foland*, 1991].

[11] The Questa porphyry Mo system is divided into three ore deposits: Spring Gulch, Central, and Log Cabin (Figure 1). The Central deposit is horseshoe shaped in map view and is the only one that is mined. Recent mining activity is underground along the southwest limb of the horseshoe ("Southwest zone"). Ore bodies are discontinuous along the Southwest zone and subdivided into the Vein zone, D ore body, and the Goat Hill ore body (Figure 2). The ore bodies within the Central deposit are mostly related to the emplacement of the Southwest intrusive suite. The Log Cabin ore body lies near the roof zone of the Bear Canyon pluton, whereas the Spring Gulch deposit lies above the Sulphur Gulch pluton. Major ore bodies at Questa are typically found at the intrusive contact with, or entirely within, pre-caldera volcanic units.

[12] The Questa ore system contains two separate styles of mineralization [*Ross et al.*, 2002]. Both the Goat Hill and D ore bodies contain disseminated molybdenite within the matrix of a magmatic hydrothermal breccia. However, the majority of the

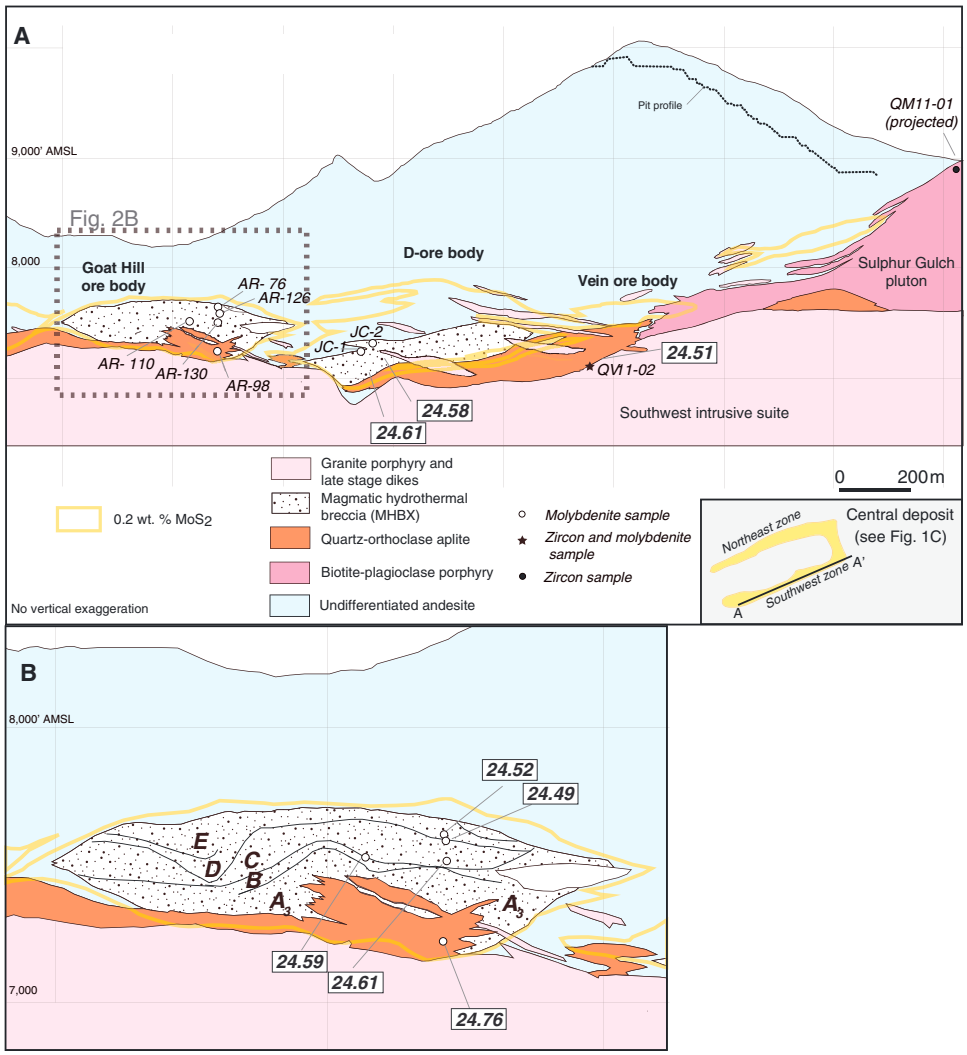

Figure 2. After *Ross et al.* [2002]. a) Simplified geologic cross section through the Southwest zone of the Central deposit (note inset, compare to Figure 1). Locations of samples from drill core that were dated by Re/Os are indicated. Numbers pointing to samples represent Re/Os molybdenite ages in Ma. Some samples are projected from nearby drill holes. b) Cross section of the Goat Hill ore body showing the semi-stratified facies (a through e) of *Ross et al.* [2002]. Numbers represent Re/Os molybdenite ages in Ma. See text for discussion.

ore is hosted within stockwork quartz + molybdenite veins. *Ross et al*. [2002] subdivided the Goat Hill hydrothermal breccia on the basis of differences in matrix paragenesis, clast alteration, and breccia textures. Consequently, they observed five semi-stratified breccia facies (a through e, Figure 2) and interpreted them to represent evolution of the hydrothermal fluid away from the source. However, fluid inclusion work shows that there was little or no correlation between fluid evolution and the breccia facies [*Rowe*, 2012].

3. Methods

3.1. U/Pb Zircon Geochronology

[13] Samples were collected from units closely associated with epithermal mineralization (Red River intrusive complex) and the porphyry Mo deposit (the Sulphur Gulch pluton, Southwest intrusive suite, and Bear Canyon pluton; Figures 1c and 2). Samples were broken down with jaw crushers and a disc mill, and either processed on a water table, sieved, or both prior to heavy liquid and magnetic mineral separation.

[14] Zircons were thermally annealed in a 950 °C oven for 48 hours, and chemically abraded in HF + HNO_3 at 220 °C for 12 hours [*Mattinson*, 2005]. The abraded zircons were spiked with a UNC in-house ^{205}Pb-^{233}U-^{236}U tracer and equilibrated in HF + HNO_3. In some cases, multigrain fractions were analyzed to counter relatively low U concentrations and the young age of these samples. After dissolution, fractions were dried and converted to chlorides. Anion exchange column chromatography was used to separate U from Pb. Uranium was loaded onto Re filaments. The majority of the U samples were loaded with graphite in order to ionize as a metal. However, several were ionized as UO_2 late in the project in an attempt to raise ionization efficiencies. There are no systematic differences in analyses that could be attributed to how U was measured. Lead was loaded with Si-gel onto zone-refined Re filaments. All analyses were made on the Daly detector of the VG Sector 54 thermal ionization mass spectrometer at the University of North Carolina — Chapel Hill. In-run U fractionations were calculated based on the measured value for $^{233}U/^{236}U$ in the spike, and Pb fractionation was assumed to be 0.15%/amu. Analyses in which U was analyzed as an oxide were corrected for oxygen isotope interferences. Raw data were processed through Tripoli [*Bowring et al*., 2011] and U/Pb Redux [*McLean et al*., 2011]. Some analyses had high total common Pb (> 3 pg) that we suspect is derived from inclusions that were not removed during chemical abrasion (e.g., fluorite). Therefore, we assumed a maximum of 3 pg blank Pb and assigned all remaining common Pb to initial sample Pb. The isotopic composition of the sample common Pb was estimated using whole-rock data from *Johnson et al*., [1990] and *Stacey and Kramers* [1975] where Pb isotope data were unavailable. All U/Pb ages are Th-corrected weighted mean ^{206}Pb-^{238}U ages. Correction for Th-disequilibrium was made using published whole-rock data for the plutons [*Johnson et al*., 1989]. The maximum Th correction was 0.085 Ma, and uncertainty in this correction is not significant for interpreting the results.

3.2. Re/Os Molybdenite Geochronology

[15] Molybdenite samples were collected from the Southwest zone of the Central deposit at Questa. We chose to date the five samples of *Rowe* [2012] and two from *Cline and Bodnar* [1994] because they determined the mineralization temperatures using fluid inclusion microthermometry for the Goat Hill and D ore bodies, respectively. The granite porphyry host for one of the samples from the Vein zone (QV11-02) was used for U/Pb zircon geochronology.

[16] Molybdenite was isolated with a diamond-tipped drill and chemically equilibrated with a mixed ^{185}Re-^{188}Os-^{190}Os spike using the *aqua regia* Carius tube method [*Shirey and Walker*, 1995]. An attempt was made to select samples that did not contain a significant amount of pyrite, although the high Re and radiogenic Os concentrations in molybdenite overwhelm any non-molybdenite Re and Os. Osmium was extracted into chloroform ($CHCl_3$) and then back extracted into HBr [*Cohen and Waters*, 1996]. Further Os purification was completed with micro-distillation [*Birck et al*., 1997] prior to being loaded onto Pt filaments with Ba $(OH)_2$. Rhenium was isolated using Cl-based anion exchange column chromatography and loaded onto Pt filaments with $Ba(NO_3)_2$. Use of $Ba(NO_3)_2$ activators permits analysis as oxide anions (N-TIMS). Measurements were made at AIRIE (Colorado State University) on a Thermo-Fisher Triton TIMS using simultaneous Faraday cup collectors for Re and stronger intensity Os signals whereas weaker Os signals were collected in peak jumping mode with a secondary electron multiplier. Both Re and Os analyses were corrected for oxygen isotope compositions, and Os was further corrected for: (1) isobaric interferences (W, Re, and Pt), (2) common Os, (3)

and mass fractionation based on the measured $^{190}Os/^{188}Os$ in the spike [*Markey et al.*, 2003]. During data reduction, Re and Os abundances were corrected for analytical blank, although blank was negligible. Ages are reported with both 2σ analytical errors and combined analytical + ^{187}Re decay constant uncertainty [*Smoliar et al.*, 1996] errors (Table 2).

4. Results

4.1. U/Pb Zircon Geochronology

[17] After Th-correction, all zircon U/Pb ages are concordant within analytical and decay constant uncertainties (Table 1 and Figure 3). Some samples show evidence for Pb-loss (e.g., JMR-34) which are identified where there are at least two outliers. A conservative age estimate was made for two samples from the Sulphur Gulch pluton (QM11-01 and JMR-6), the sample from the Bear Canyon pluton (JMR-34), and one from the Red River intrusive complex (MZQ-5) because they revealed a continuum of ages that could be related to inheritance, Pb loss and/or protracted zircon growth.

[18] A granite porphyry (MZQ-5) and equigranular granodiorite (JMR-5) were collected from the southern and central portion of the composite Red River intrusive complex, respectively. Five zircon fractions from the granite porphyry yield a weighted mean $^{206}Pb/^{238}U$ age of 25.21 ± 0.055 Ma (N = 5; MSWD = 5.5). Four of the five fractions overlap within uncertainty. All four fractions analyzed from the granodiorite phase of the Red River pluton agree within uncertainty and define a weighted mean age that is identical to the granite porphyry (25.20 ± 0.036; MSWD = 0.79).

[19] A sample of the biotite-plagioclase aplite porphyry (sample QM11-01) of the Sulphur Gulch pluton was collected from within the open pit mine in the Central deposit. This sample yields a weighted mean age with statistically significant scatter (24.91 ± 0.069; $N = 8$; MSWD = 14). The second sample from the Sulphur Gulch pluton is a non-mineralized granite porphyry (JMR-6). The interpreted age for this sample is 24.44 ± 0.086 Ma ($N = 9$; MSWD = 11).

[20] A mineralized (pyrite and molybdenite) granite porphyry from the Vein zone orebody of the Southwest intrusive suite yields an age of 24.53 ± 0.045 Ma (MSWD = 8.3).

[21] Sample JMR-34 from the Bear Canyon pluton yielded zircons that were generally larger and more euhedral than those from more altered samples (e.g., Sulphur Gulch). Two fractions from this sample are significantly younger than the other analyses could possibly reflect Pb loss. However, we included all analyzed fractions, which yields weighted mean age of 24.46 ± 0.050 Ma (MSWD = 10.3).

4.2. Re/Os Molybdenite Geochronology

[22] Five vein-hosted and three breccia matrix molybdenite samples were analyzed from three separate ore bodies within the Central deposit (Goat Hill, D, and Vein; Table 2, Figure 4). All samples have moderate Re concentrations (< 70 ppm), and there is no correlation of Re concentration with mineralization style or ore body.

[23] The oldest molybdenite age obtained in this study is 24.76 ± 0.026 Ma from a quartz + molybdenite vein hosted in the aplite beneath the Goat Hill ore body. Two breccia matrix-hosted molybdenite samples yield analytically distinct ages of 24.61 ± 0.028 and 24.49 ± 0.043 Ma. Two vein-style molybdenite veins from within the same Goat Hill ore body yield ages of 24.59 ± 0.026 and 24.52 ± 0.028 Ma.

[24] Two samples from the D ore body yield ages of 24.61 ± 0.028 and 24.58 ± 0.027 Ma for vein and breccia matrix-hosted mineralization styles, respectively. One molybdenite vein that cuts granite porphyry within the Vein ore body was selected for both Re/Os molybdenite and U/Pb zircon geochronology. This sample yields a Re/Os age of $24.51 \pm 0.032/0.085$ Ma (uncertainties corresponding to analytical, and analytical with ^{187}Re decay constant error, respectively) which is within uncertainty of the U/Pb zircon age obtained for the host granite (24.53 ± 0.052 Ma).

5. Discussion

[25] Combining U/Pb zircon geochronology of intrusive rocks with Re/Os molybdenite ages from the Questa Mo deposit allows us to characterize the timing and duration of magma emplacement with respect to mineralization. Additionally, most of the samples used for Re/Os geochronology were analyzed for mineralization temperatures in earlier studies [*Cline and Bodnar*, 1994; *Rowe*, 2012], thus permitting combination of the new ages with temperature data to evaluate Re/Os as a thermochonometer. All the data can be considered within the framework of the evolution of the host Latir

Table 1. U-Pb Data for Caldera Margin Rocks from the Latir Volcanic Field

Sample Fraction (n)	U (ppm)	Pb[a] (pg)	Th[b] / U	^{206}Pb[c] / ^{204}Pb	^{206}Pb[d] / ^{238}U	Error (%)	^{207}Pb[d] / ^{235}U	Error (%)	^{207}Pb[d] / ^{206}U	Error (%)	Ages (Ma)[e] ^{206}Pb / ^{238}U	Ages (Ma)[e] ^{207}Pb / ^{235}U	Ages (Ma)[e] ^{207}Pb / ^{206}U	Corr. Coeff.	Total[f] Common Pb (pg)
JMR-5 Granodiorite; Red River Intrusive Suite (Th/U = 3.3: 464347, 4064398)[g]															
F-1 (1)	149	7	1.20	195	0.0039161	0.68	0.026268	6.6	0.048649	6.2	25.26	26.33	130.9	0.542	2.1
F-2 (1)	99	15	1.29	720	0.0039043	0.15	0.025407	1.6	0.047196	1.6	25.19	25.48	59.2	0.619	1.1
F-3 (1)	126	6	1.15	169	0.0039110	0.77	0.025755	7.0	0.047761	6.6	25.23	25.82	87.5	0.550	2.1
F-4 (1)	133	13	1.10	259	0.0039146	0.43	0.025191	3.9	0.046672	3.7	25.26	25.26	32.5	0.516	2.7
MZQ-5 Granite Porphyry; Red River Intrusive Suite (Th/U = 4.97: 455754, 4701203)															
F-4 (2)	432	19	0.85	691	0.0038956	0.12	0.025371	1.6	0.047235	1.5	25.15	25.44	61.1	0.666	1.6
F-6 (4)	1004	44	0.81	1323	0.0039072	0.10	0.025405	0.9	0.047158	0.8	25.23	25.47	57.2	0.615	1.9
F-8 (4)	766	35	0.92	243	0.0039113	0.23	0.025557	2.7	0.047390	2.5	25.25	25.62	68.9	0.720	8.3
F-10 (4)	406	39	1.23	207	0.0039146	0.26	0.025940	3.6	0.048060	3.4	25.27	26.00	102.2	0.700	10.5
F-12 (2)	130	12	0.92	390	0.0038997	0.19	0.025060	3.1	0.046607	2.9	25.18	25.13	29.1	0.726	1.7
QM11-01 Biotite-Plagioclase Porphyry; Sulphur Gulch Pluton (Th/U = 3.8: 454580, 4062090)															
F-2 (3)	230	59	0.75	1237	0.0038379	0.15	0.024676	0.9	0.046631	0.8	24.78	24.75	30.4	0.553	2.8
F-3 (2)	101	41	0.95	393	0.0038498	0.18	0.025054	1.8	0.047199	1.7	24.85	25.13	59.3	0.546	5.9
F-4 (1)	197	68	0.77	1896	0.0038688	0.14	0.024942	0.6	0.046758	0.6	24.98	25.01	36.9	0.466	2.1
F-6 (2)	194	25	0.79	800	0.0038608	0.12	0.025160	1.4	0.047265	1.4	24.93	25.23	62.6	0.633	1.8
F-7 (1)	299	13	0.66	119	0.0038640	0.37	0.025565	6.1	0.047986	5.9	24.95	25.63	98.6	0.599	7.3
F-8 (1)	202	9	0.86	307	0.0038765	0.25	0.025256	3.9	0.047253	3.7	25.03	25.33	62.0	0.759	1.7
F-9 (1)	266	23	0.87	288	0.0038541	0.21	0.025164	2.5	0.047352	2.4	24.88	25.23	67.0	0.612	4.8
F-10 (1)	70	7	1.04	209	0.0038803	0.41	0.024795	6.4	0.046344	6.1	25.04	24.87	15.5	0.822	1.9
QV11-02 Granite Porphyry; Southwest Intrusive Suite (Th/U = 3.8: Drill Hole 36.5–54.5, 62')															
F-1 (4)	334	42	0.74	1928	0.0038087	0.13	0.024621	0.6	0.046883	0.6	24.59	24.70	43.3	0.498	1.3
F-2 (4)	351	71	0.61	3440	0.0037930	0.10	0.024486	0.4	0.046820	0.4	24.50	24.56	40.0	0.614	1.2
F-3 (3)	427	69	0.61	2203	0.0037978	0.17	0.024509	0.6	0.046805	0.5	24.53	24.59	39.3	0.497	1.9
F-4 (5)	296	36	0.63	1489	0.0037951	0.11	0.024567	0.8	0.046948	0.8	24.51	24.64	46.6	0.544	1.5
F-5 (1)	228	55	0.58	1163	0.0038097	0.14	0.024563	0.7	0.046762	0.7	24.60	24.64	37.1	0.480	2.9
F-6 (1)	73	3	0.68	194	0.0037746	0.38	0.024690	6.3	0.047441	6.0	24.38	24.77	71.5	0.777	1.0
F-7 (1)	164	13	0.63	353	0.0037887	0.30	0.024755	2.8	0.047388	2.7	24.47	24.83	68.8	0.522	2.4
F-8 (2)	84	10	0.61	214	0.0037919	0.37	0.024300	4.2	0.046478	4.0	24.49	24.38	22.5	0.564	3.1
JMR-34 Granite Porphyry; Bear Canyon Pluton (Th/U = 4.0: 450594, 4060825)															
F-1 (2)	179	15.0	0.73	584	0.0037927	0.13	0.024589	0.8	0.047020	0.7	24.49	24.67	50.3	0.666	1.5
F-3 (2)	232	9.5	0.69	304	0.0037617	0.21	0.024086	2.3	0.046437	2.2	24.29	24.17	20.4	0.429	2.0
F-4 (2)	270	22.5	0.74	228	0.0037711	0.24	0.024084	2.3	0.046319	2.2	24.35	24.16	14.3	0.626	6.1
F-5 (4)	596	120.4	0.60	3629	0.0037899	0.09	0.024392	0.2	0.046677	0.2	24.48	24.47	32.8	0.691	2.0
F-6 (4)	254	63.1	0.70	2501	0.0037907	0.10	0.024384	0.3	0.046653	0.2	24.48	24.46	31.5	0.783	1.5
F-7 (2)	388	47.4	0.64	628	0.0037859	0.15	0.024480	0.8	0.046895	0.7	24.45	24.56	43.9	0.559	4.5
F-8 (4)	343	41.8	0.62	946	0.0037874	0.17	0.024522	0.5	0.046960	0.5	24.46	24.599	47.2	0.614	2.7
JMR-6 Granite Porphyry; Sulphur Gulch Pluton (Th/U = 3.8: 455776, 4060997)															
F-1 (3)	129	5.4	0.75	185	0.0037740	0.55	0.024032	4.5	0.046184	4.2	24.37	24.11	7.2	0.538	1.8
F-2 (2)	246	10.3	0.72	164	0.0038136	0.39	0.024948	4.0	0.047446	3.8	24.63	25.02	71.7	0.623	4.0

Geochemistry Geophysics Geosystems G3

10.1002/ggge.20048

Table 1. (continued)

									Ages (Ma)[e]				Total[f]
F-3 (4)	442	17.6	0.55	288	0.0037924	0.23	0.024808	2.2	0.047443	2.0	24.49	24.88	71.6	0.614	3.9
F-5 (1)	500	6.4	0.79	387	0.0038059	0.22	0.024951	3.1	0.047547	2.9	24.57	25.02	76.8	0.736	1.0
F-7 (1)	528	20.9	0.52	1303	0.0037868	0.25	0.024463	0.9	0.046852	0.8	24.46	24.54	41.7	0.452	1.0
F-8 (1)	704	5.9	0.80	376	0.0037550	0.24	0.024911	3.2	0.048116	3.0	24.25	24.98	105.0	0.749	0.9
F-9 (3)	162	54.3	0.76	1573	0.0037770	0.17	0.024281	0.7	0.046624	0.6	24.39	24.36	30.0	0.643	2.0
F-11 (3)	358	14.6	0.64	252	0.0037843	0.29	0.024602	2.9	0.047150	2.7	24.44	24.68	56.8	0.679	3.6
F-12 (3)	412	16.2	0.49	611	0.0038016	0.75	0.024466	2.2	0.046675	1.7	24.56	24.54	32.6	0.746	1.7

[a]Total mass of radiogenic Pb.
[b]Th contents calculated from radiogenic ^{208}Pb and the $^{207}Pb/^{206}Pb$ date of the sample, assuming concordance between U-Th and Pb systems.
[c]Measured ratio corrected for fractionation and spike contribution only.
[d]Measured ratios corrected for fractionation, tracer, blank, and initial common Pb.
[e]Th-corrected isotopic dates calculated using the decay constants $\lambda_{238} = 1.55125E^{-10}$ and $\lambda_{235} = 9.8485E^{-10}$ [*Jaffey et al.*, 1971].
[f]Total mass of common Pb.
[g]Locations in NAD 27, UTM Zone 13.
Lab blank assumed to be 2 ± 1 pg.
Initial Pb for samples QV11-02, QM11-01, and QM11-04 use Stacey and Kramers (1975) at 25 Ma. All others use data from Johnson et al. (1990).
Pb blank ratios: $^{206}Pb/^{204}Pb = 18.864 \pm 0.25$; $^{207}Pb/^{204}Pb = 15.630 \pm 0.25$; $^{208}Pb/^{204}Pb = 38.193 \pm 0.50$ (1-sigma).

volcanic field to develop a model for porphyry Mo mineralization.

5.1. Intrusive History of the Caldera Margin Plutons

[26] The Red River intrusive complex is the oldest and easternmost of the caldera margin plutons. Equigranular granodiorite exposed in the central portion of the pluton was previously interpreted as the remnant magma chamber of a pre-caldera andesitic volcano [*Lipman*, 1988; *Lipman and Reed*, 1989]. However, the geochronologic data presented here indicate that the granodiorite crystallized approximately 300 ka after the eruption of the Amalia Tuff, nearly concurrently with high-silica granitic magma at ~25.20 Ma (Figure 5). However, field relations demonstrate that the Red River granite is part of a dike swarm that crosscuts the granodiorite [*Lipman and Reed*, 1989]. Therefore, although the units are the same age within uncertainty, the granite is demonstrably younger.

[27] *Johnson et al*. [1989] used major and trace element modeling to determine that the granodiorite within the Red River intrusive complex could not be a parental magma for the high silica aplite, thereby limiting the possibility that these magmas represent a single differentiated intrusion. Instead, the Red River pluton appears to have been assembled rapidly by intrusion of compositionally diverse magma pulses around 25.20 Ma.

[28] Following intrusion of the Red River intrusive complex, magmatism moved westward. New U/Pb zircon ages presented here suggest that the Sulphur Gulch pluton was assembled between 24.91 and 24.44 Ma with the biotite-plagioclase porphyry predating the granitic phase of the pluton. The granitic phases of the Sulphur Gulch pluton, Southwest intrusive suite and Bear Canyon pluton all intruded within uncertainty of each other at ~24.50 Ma. These high-silica granites were the primary contributors of metal-rich brines that resulted in breccia matrix-hosted and stockwork-style mineralization [*Cline and Bodnar*, 1994; *Ross et al*., 2002; *Klemm et al*., 2008; *Rowe*, 2012].

[29] Field mapping and gravity anomaly data indicate that the southern caldera margin plutons are upper portions of a partial ring intrusion along the caldera margin [*Cordell et al*., 1985; *Lipman et al*., 1986; *Meyer*, 1991]. The U/Pb zircon geochronologic data presented here indicate that assembly occurred over ~770 ka. We interpret the age range

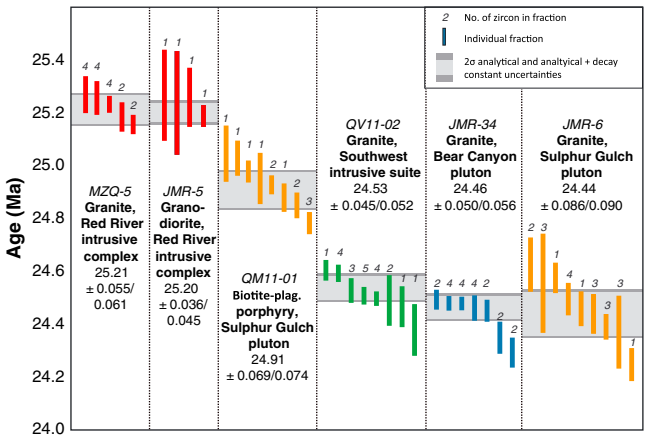

Figure 3. $^{206}Pb/^{238}U$ ages for individual analyses. Vertical bars correspond to 2σ analytical uncertainties for individual analyses. Horizontal bars represent the weighted mean age with analytical uncertainty only. Ages in text are in Ma with analytical/analytical + decay constant uncertainties. For comparison of U/Pb ages to each other, error bars without decay constant uncertainties are relevant. For comparison of U/Pb ages to Re/Os and Ar/Ar ages, decay constant uncertainties in each system must be considered.

to represent a minimum assembly interval because thermal modeling demonstrates that crystallization of such a small magma volume would have occurred an order of magnitude more quickly [*Spera*, 1980]. This period corresponds to only a small interval of the ~6 Ma post-caldera pluton assembly history for the entire region [*Tappa et al*., 2011; *Zimmerer and McIntosh*, 2012], but brackets the time in which major magmatic hydrothermal systems were active [*McLemore and North*, 1984; *Lipman et al*., 1986; *Lipman*, 1988; *Meyer and Foland*, 1991; *Ross et al*., 2002]. These data are consistent with *Zimmerman et al*. [2008], who observed that major porphyry-style mineralization episodes are short-lived relative to their host magmatic districts.

5.2. History of Mineralization

[30] Numerous occurrences of epithermal Au-Ag veins are present within the Red River intrusive complex and its wallrocks [*McLemore and North*, 1984]. New ages presented here therefore place a maximum age of 25.20 Ma on the epithermal-style mineralization. A younger age for mineralization cannot be ruled out; however, the epizonal textures associated with the pluton [*Lipman*, 1988] suggest that minor epithermal Au-Ag mineralization was synchronous with pluton assembly.

[31] Field evidence and fluid inclusion analysis [*Rowe*, 2012] demonstrate that the Mo mineralization at Questa involved multiple events and hydrothermal fluids. Major molybdenite mineralization at Questa was coeval with the emplacement of the Southwest intrusive suite, and the Sulphur Gulch and Bear Canyon plutons. The earliest mineralizing intrusion identified in this study is the biotite-plagioclase porphyry of the Sulphur Gulch pluton (24.91 ± 0.069 Ma) which is exposed in the open pit, just east of the Central ore body. The open pit mine, which is no longer active, targeted lode-style molybdenum mineralization [*Ross et al*., 2002] which probably received its metals from this intrusion. Generally, local ore grades are highest sub-parallel to the contact between the biotite-plagioclase porphyry and the pre-caldera andesite [*B. Walker*, per. comm.]. These field relationships suggest that this intrusion contributed ore to the system rather than acting as a host for later mineralization events.

[32] Molybdenite Re/Os ages record 250 ka of mineralization in perhaps three episodes (Figure 4). These data reflect the minimum duration of molybdenite mineralization because we targeted samples with independent temperature estimates rather than initial and final events. Seven of the eight molybdenite samples have ages between ~24.6 and 24.5 Ma, suggesting that major mineralization event occurred over this time interval. During this time period, both breccia matrix- and vein-style ore were deposited within the Goat Hill and D ore bodies [*Ross et al*., 2002]. These data demonstrate that the two distinct styles of mineralization were coeval in space and time for ~100 ka.

[33] The Goat Hill ore body alone was mineralized over a period of 250 ka, and molybdenite Re/Os ages become progressively younger upsection through its semi-stratified facies [Figure 2b; *Ross et al*., 2002]. These data could reflect time-progressive fluid evolution away from the source intrusion [*Ross et al*., 2002], but that requires the hydrothermal system to

Table 2. Re-Os Data for Molybdenite of the Questa Porphyry Mo Deposit

AIRIE	Sample	Drill			%	Re	±	^{187}Os	±	Comm.	Age	±2σ	±2σ
Run #[a]	Name	Hole	Description[b]	Ore Body	Moly[c]	(ppm)	2σ	(ppb)	2σ	Os (ppb)[d]	(Ma)[e]	anal.[f]	anal. + λ^f
MD-1254	AR-98	22.0–14.0	Vein in aplite	Goat Hill	80	22.20	0.015	5.758	0.0048	0.012	24.760	0.026	0.083
MD-1255	AR-110	23.4–11.8G	Vein in MHBX facies A_3	Goat Hill	70	45.24	0.030	11.653	0.0095	0.041	24.594	0.026	0.083
MD-1299	AR-130	22.0–14.0	MHBX facies C	Goat Hill	100	30.64	0.025	7.897	0.0065	0.000	24.612	0.028	0.084
MD-1265	AR-76	22.0–14.0	Vein in MHBX facies D	Goat Hill	100	38.99	0.031	10.013	0.0084	0.000	24.520	0.028	0.083
MD-1296	AR-126	22.0–14.0	MHBX facies D	Goat Hill	30	1.894	0.0029	0.4858	0.0004	0.000	24.490	0.043	0.090
MD-1295	JC-1	28.9–25.5HA	Vein	D	20	6.553	0.0052	1.689	0.0014	0.000	24.606	0.028	0.084
MD-1298	JC-2	28.9–25.5HA	MHBX	D	70	39.03	0.028	10.046	0.0081	0.016	24.579	0.027	0.083
MD-1308	QV11-02	36.5–54.5 VN20	Vein	Vein zone	90	26.39	0.027	6.775	0.0055	0.000	24.514	0.032	0.085

Carius tube dissolution and sample-spike equilibration using a mixed-double Os spike *Markey et al.* [2003] with sample weights 21–33 mg. All data are blank corrected, and Os isotopic measurements are fractionation corrected (using the double Os spike).

[a]AIRIE run # refers to internal lab designation common to all AIRIE samples.

[b]MHBX = Magmatic-hydrothermal breccia. Facies correspond to those of *Ross et al.* [2002].

[c]Percent molybdenite in drilled separate is based on a visual estimate under the binocular microscope. No other sulfides observed. Quartz-feldspar-biotite dilutant does not affect Re-Os age calculation.

[d]Common Os is insignificant to the age calculation, and essentially zero for all analyzed molybdenites.

[e]For MD-1254, MD-1255, MD-1256, Re blank = 24.22 ± 0.15 pg, total Os = 2.00 ± 0.02 pg with $^{187}Os/^{188}Os = 0.231 \pm 0.001$. For MD-1295, MD-1296, MD-1298, MD-1299, MD-1308, Re blank = 7.85 ± 1.48 pg, total Os = 1.86 ± 0.03 pg with $^{187}Os/^{188}Os = 0.322 \pm 0.010$.

[f]Uncertainty on ages shown for both analytical error, and combined analytical and decay constant uncertainty for ^{187}Re errors (0.31%, *Smoliar et al.*, 1996).

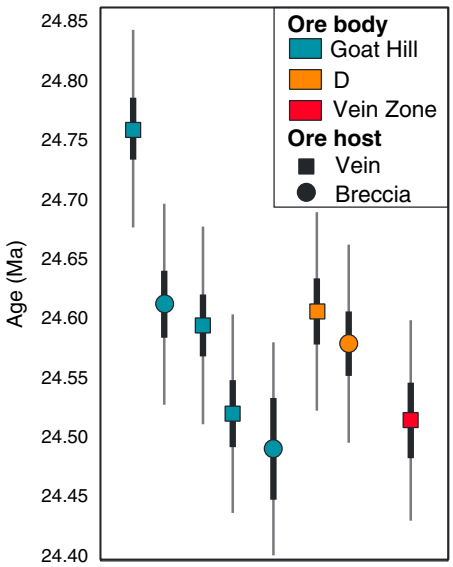

Figure 4. Molybdenite Re/Os ages for various ore bodies. Error bars correspond to 2σ analytical uncertainties (thick, bold lines) and analytical + decay constant uncertainty (thin gray lines — see caption for Figure 3 for appropriate use of uncertainties). Vein and breccia represent vein- and breccia-matrix hosted mineralization styles, respectively. Note that decay constant uncertainties are only needed when comparing to other geochronometers (e.g., U/Pb).

have been active for hundreds of thousands of years. This is unlikely given the short lifespan predicted by numerical models for an intrusion the size of the source (< 1 km^3; *Cathles et al.*, 1997; *Ross et al.*, 2002). *Ross et al.* [2002] noted that numerous dikes emanate from the roof of the aplite below the Goat Hill ore body. These intrusions may have been diachronous rather than extensions of a single intrusion, thereby allowing the possibility that the source aplite represents a series of amalgamated dikes. It is proposed that initial brecciation created an isotropic zone of weakness that re-fractured episodically during subsequent dike intrusions and fluid exsolution over a prolonged time period. Essentially, the Goat Hill hydrothermal breccia may have acted as a small trap that was easily shattered, thereby depressurizing small intrusions and favoring magma quenching and fluid exsolution [*Candela*, 1997].

[34] *Burnham* [1997] suggests that the presence of multiple populations of stockwork veins within porphyry-type systems could be related to the interplay between downward crystallization and repetitious crack-seal events within a single magma chamber. However, the total duration of Re/Os molybdenite ages observed in this study is too long for such a simplified process. It is proposed here that each mineralization stage corresponds to a complete cycle

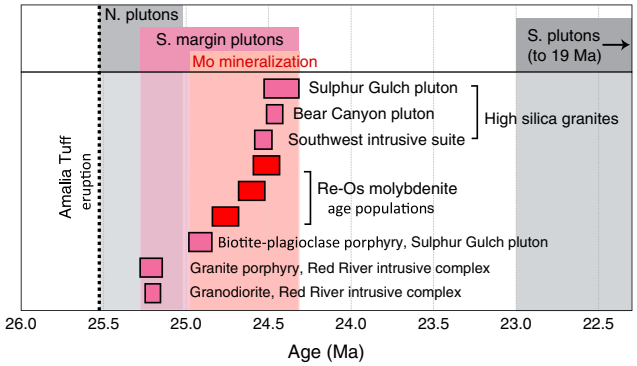

Figure 5. Summary of U/Pb and Re/Os geochronology for the volcanic and plutonic rocks related to the Questa-Latir volcanic field after the eruption of the Amalia Tuff. Purple (U/Pb zircon) and red (molybdenite Re/Os) blocks represent new data from this study. Block width represents 2σ uncertainty, including decay constant uncertainty. N. plutons = northern plutons (Cabresto Lake, Virgin Canyon, Cañada Pinabete, and Rito del Medio; Figure 1b). S. plutons = Southern plutons (Rio Hondo and Lucero Peak; Figure 1b). Total duration of mineralization includes the emplacement age of the biotite-plagioclase porphyry phase of the Sulphur Gulch pluton.

of magma injection, fluid exsolution, circulation, cooling, and mineralization. These data substantiate previous interpretations that Climax-type deposits form via complex multi-phase mineralization [*Wallace et al*., 1968; *Seedorff and Einaudi*, 2004a].

[35] In all, our data indicate syn-mineralization pluton emplacement over a period of about 770 ka (Red River intrusive complex through high-silica granite phase of Sulphur Gulch pluton) with early Au-Ag mineralization followed by at least 250 ka (and perhaps 400 ka if mineralization of the biotite-plagioclase porphyry was synchronous with intrusion) of Mo mineralization. Variable textures throughout caldera margin plutons with discrete intrusive contacts indicate at least a portion of the system was assembled by injection of numerous small intrusions. These data are consistent with growing body of evidence for incremental pluton assembly [e.g. *Coleman et al*., 2004; *Matzel et al*., 2006; *Davis et al*., 2012; *Tappa et al*., 2011; *Leuthold et al*., 2012], and links this concept with models for episodic porphyry mineralization [*Wallace et al*., 1968; *Carten et al*., 1988a; *Maksaev et al*., 2004; *Seedorff and Einaudi*, 2004a; *Wilson et al*., 2007].

5.3. Re/Os Molybdenite: A New Thermochronometer

[36] If molybdenum mineralization is demonstrably related to magma emplacement, such as in porphyry ore systems, the mineralization temperature can be used to help construct a system-wide thermal history. Fluid inclusion studies reveal that mineralization within porphyry systems occurs at temperatures between ~300 and 500 °C, with modes typically ~400 °C [*Cline and Bodnar*, 1994; *Selby et al*., 2000; *Klemm et al*., 2008; *Rowe*, 2012]. Because thermal modeling [e.g., *Hanson and Glazner*, 1995; *Yoshinobu et al*., 1998] demonstrates that incrementally assembled plutons "dwell" in the temperature window between hornblende and biotite Ar closure temperatures [~ 525 °C and ~325 °C, respectively; *Harrison*, 1981; *Harrison et al*., 1985], Re/Os molybdenite data can fill an important gap in our understanding of these systems [e.g., *Stein et al*., 2001; *Markey et al*., 2003].

[37] Most of the molybdenite separates used in this study are extracted from the same samples that were used in fluid inclusion studies, thereby allowing correlation of microthermometry results and Re/Os molybdenite ages. For the Goat Hill ore body, *Rowe* [2012] determined a primary mineralization stage to occur at 380 °C, with another significant stage at ~280 °C. *Rowe* [2012] observed evidence for halite trapping (e.g., multiple halite crystals in one inclusion), and as a result she reported liquid-vapor homogenization temperatures. This is in contrast to the studies from the D ore body [*Cline and Bodnar* 1994; *Klemm et al*. 2008], for which halite homogenization temperatures are reported. Both of these studies determined mineralization temperatures to be > 410 °C for the D ore body. Because halite typically dissolves at a higher temperature than liquid-vapor homogenization in fluid inclusions from porphyry ore systems [e.g. *Becker et al*., 2008], the difference in temperature estimates between the Goat Hill and D ore bodies is likely minimal. Consequently, we use an intermediate temperature of ~400 °C for our discussion.

[38] The dispersion of Re/Os molybdenite ages presented here is interpreted to reflect episodic

mineralization events. Therefore, chronologically later mineralization episodes with temperatures on the order of 400 °C did not disturb the Re/Os system in molybdenite. This observation is consistent with previous studies where Re/Os molybdenite ages were not reset by high-grade metamorphism [*Stein et al.*, 1999, 2001, 2003; *Stein and Bingen*, 2002; *Stein*, 2006], and discrete Re/Os molybdenite ages that are concordant with U/Pb zircon ages from associated intrusions [*Selby et al.*, 2007; *Maksaev et al.*, 2004]. These data also support previous work that predicts the closure temperature of the Re/Os system in molybdenite to be > 400 °C [*Suzuki et al.*, 1996]. As a result, Re/Os molybdenite is considered a useful new thermochronometer in geologic settings where molybdenite is the primary sulfide phase.

5.4. Integrated T-t History of the Questa Porphyry System

[39] Combination of new U/Pb and Re/Os ages allows evaluation of the T-t history of the caldera margin plutons and mineralization. Uncertainties in ages in this section include propagation of full analytical uncertainties and ^{238}U and ^{187}Re decay constant uncertainties. The geochronologic data place magmatic-hydrothermal mineralization along the Red River valley into a period of relatively low magma flux that existed following the eruption of the Amalia Tuff [*Tappa et al.*, 2011]. Additionally, the timing of Mo mineralization is bracketed by the zircon ages of spatially associated plutons. Individual cycles of magma emplacement, fluid exsolution, and mineralization were short-lived from zircon saturation (~ 750 °C) through molybdenite mineralization (~ 400 °C). Consider sample QV11-02 from the Vein ore body (Figures 2 and 6a). Zircon crystallization within this sample occurred at 24.53 ± 0.052 Ma, and the pluton is cut by a molybdenite vein, dated at 24.51 ± 0.085 Ma. It is possible that molybdenite from the vein was not sourced from the same intrusive rock that was sampled; regardless, these data limit the duration of time between zircon crystallization and brittle-vein formation to have occurred within uncertainty of the ages, consistent with rapid cooling.

[40] Acknowledging these rapid cooling rates allows for a general interpretation of thermal cycling within the system (Figure 6b). Note, however, that our sampling strategy targeted samples where independent

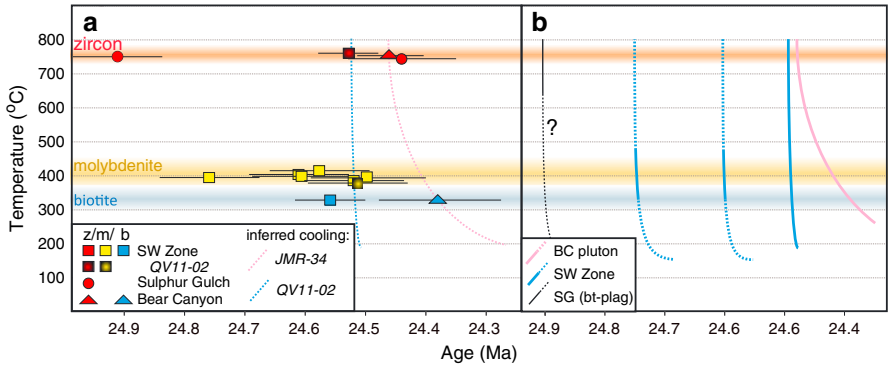

Figure 6. a) T-t plot showing crystallization ages of plutons related to molybdenite mineralization within the Questa ore system. "z/m/b" indicates symbols for zircon/molybdenite/biotite. Yellow horizontal band corresponds to uncertainties in molybdenite precipitation temperature (see text). Zircon U/Pb saturation temperature was calculated using whole rock data of *Johnson et al.* [1989] and equations of *Watson and Harrison* [1983]. Data for this calculation were available for all intrusions except the Southwest intrusive suite. We used the data for the modally similar Sulphur Gulch pluton to calculate zircon saturation temperature for this sample. Biotite closure temperature from *Harrison et al.* [1985]. Horizontal error bars represent 2σ uncertainties (including decay constant uncertainties, except for Ar/Ar ages, which have external uncertainties ~ 1 Ma). Note that some samples are offset on the *y*-axis for clarity and not because of measurable differences in temperature. The Ar/Ar age for the high-silica phase of the Sulphur Gulch granite has been omitted for clarity (24.73 ± 0.14/0.98 Ma; *Zimmerer and McIntosh*, 2012). b) Interpreted thermal history based on data in part A. Solid lines represent cooling periods as defined by geochronology where U/Pb zircon data are complimented by a low-T chronometer, whereas dotted lines are inferred. Dotted lines were placed by transposing the rapid cooling rate of the Southwest and Bear Canyon plutons back in time. Cooling curve for sample JMR-6 (high-silica granite of the Sulphur Gulch pluton) was excluded for clarity; however, *Zimmerer and McIntosh* (2012) demonstrated that this intrusion followed a much more simple cooling path than the Bear Canyon pluton. Note that three molybdenite populations were identified from Re/Os molybdenite ages without decay constant uncertainties. The added uncertainties only change what intrusion could be paired with the molybdenite age, not their internal differences.

determinations of temperature were available and therefore may exclude higher frequency events. Identifying more equivalent U/Pb zircon and Re/Os molybdenite ages, such as those demonstrated for sample QV11-02, would strengthen this hypothesis. However, our sampling strategy was largely limited to samples previous fluid inclusion studies [*Cline and Bodnar*, 1994; *Rowe*, 2012], many of which do not contain enough material for U/Pb zircon analysis. Regardless, the combination Re/Os molybdenite and U/Pb zircon geochronology for sample QV11-02 demonstrate that, where available, such relationships can be identified. Thus, we infer multiple thermal cycles over 250 ka wherein each hydrothermal circulation event corresponds to a specific intrusion that cools rapidly [*Cathles et al*., 1997; blue line, Figure 6b].

[41] Evidence for rapid cooling from igneous through hydrothermal conditions is consistent with numerical models for shallow magmatic systems such as the one responsible for mineralization at Questa [3–5 km at time of emplacement; *Cline and Bodnar*, 1994; *Cathles et al*., 1997]. These data add to a growing body of evidence that suggest porphyry ore systems are characterized by multiple injections of magma where each pulse creates a hydrothermal circulation cell that remains active for < 100 ka [*Marsh et al*., 1997; *Maksaev et al*., 2004; *Lawley et al*., 2010; *Braxton et al*., 2012]. However, this study is the first to provide the timing and duration of multiple cycles for a Climax-type porphyry Mo system, and we suggest that individual cycles are possibly active for very short times (within uncertainty of the chronometers in this study).

5.5. Evaluation of Previous Genetic Models for the Questa Mo Deposit

[42] Previous thought on the origin of the Questa porphyry Mo deposit calls upon (1) chemical differentiation processes (assimilation, crystal fractionation, volatile fluxing) in a long-lived magma chamber within the middle to upper crust [*Johnson et al*., 1989; *Carten et al*., 1993] or (2) fractional crystallization in the lower crust [*Klemm et al*., 2008]. The mineralizing intrusions in these cases are believed to be cupolas that emanate from these long-lived reservoirs. Detailed geo-thermochronology presented here challenges these hypotheses.

[43] Agreement of U/Pb zircon ages with Re/Os molybdenite geochronology for the suite of high-silica granites precludes the possibility that these intrusions resided in a long-lived upper crustal magma chamber [e.g. *Johnson et al*., 1989; *Carten et al*., 1993]. Any fractionating chamber would have been below zircon saturation temperatures (750° to 780 °C) and crystallizing zircon [*Johnson et al*., 1989]. This predicts a gap between zircon saturation and cooling coincident with intrusion and mineralization (Figure 7a). Mafic recharge into the base of the system could reheat it above zircon saturation temperatures [e.g. *Carten et al*., 1993]; however, this requires a significant volume of mafic magma that is unrecognized in surface and subsurface data [*Lipman and Reed*, 1989; *Meyer*, 1991; *SRK Consulting*, *Inc. report*].

[44] Alternatively, in situ magma differentiation could take place in the deep crust where ambient temperatures are higher. *Klemm et al*. [2008] suggested that ~95% crystallization of a middle to lower crustal magma chamber is required to explain the rapid increase in Cs concentration within hydrothermal fluids between breccia matrix-style and vein-style mineralization. However, the Re/Os molybdenite ages in this study clearly show that these mineralization styles were concurrent over a ~100 ka period. Therefore, the data of *Klemm et al*. [2008] cannot represent a time-progressive geochemical trend.

[45] The repetitious intrusion of mineralizing granitic magmas and the synchroneity of high- and low-temperature thermochronometers favors an evolution model in which the magmas are generated, ascend, and cool quickly (Figure 7b). We propose that, like other magmas associated with the Latir field, the origin of the mineralizing magmas was the lower crust [*Johnson et al*, 1990; *Tappa et al*., 2011].

5.6. Relationship Between Caldera Formation and Mineralization

[46] An intriguing set of observations from the detailed geochronology now available for the Latir volcanic field is that high-silica granites capable of mineralization were emplaced within only 0.25–0.40 Ma of the total 8.5 Ma history of the Latir field (~ 28.5 to 19.1 Ma; *Zimmerer and McIntosh* [2012]) and that this short episode of mineralization occurred immediately after the eruption of the caldera-forming Amalia Tuff (~ 25.52 Ma, *Tappa et al*. [2011]). Numerous authors discuss the relationship between large-volume calderas and their control on mineralization [e.g., *Lipman*, 1992; *Rytuba*, 1994; *Henry et al*., 1997; *Singer and Marchev*, 2000]; however, the majority of the discussion is centered on structural controls related to caldera subsidence (e.g. ring faults) and

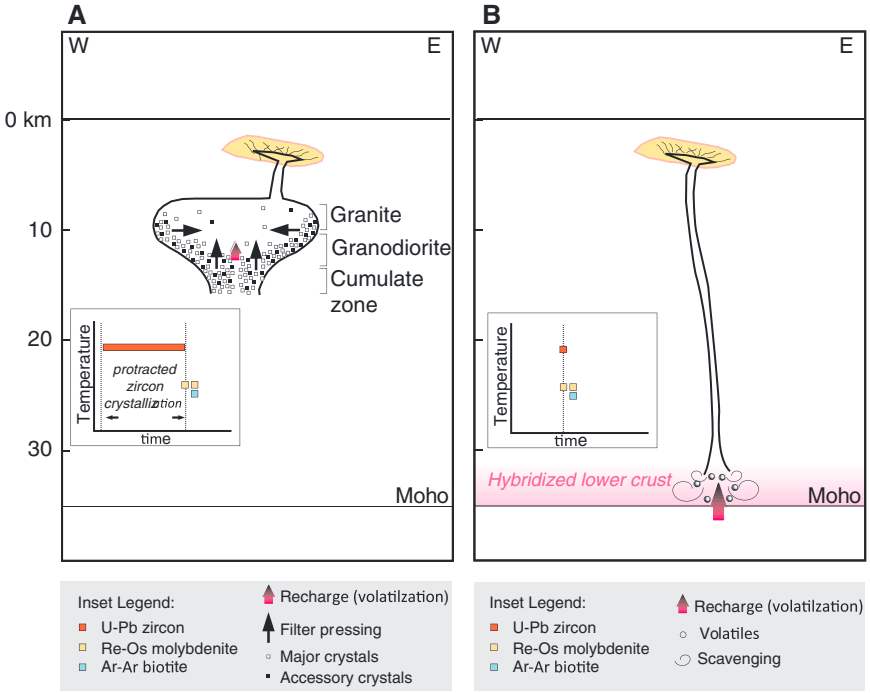

Figure 7. Schematic drawings showing general differences between expected T-t distribution across multiple chronometers (insets) for different magma evolution settings along an E-W cross-section through the southern caldera margin. a) Crystal fractionation model with variable recharge (modified from *Johnson et al*., 1989; *von Quadt et al*., 2011) in a vertically extensive mid- to upper-crust magma chamber. Mineralizing cupolas emanate from the upper crustal reservoir and ultimately crystallize and exsolve hydrothermal fluids in the shallow crust. The presence of a long-lived magma chamber in the upper crust predicts that zircon begins to crystallize at a much earlier time than low-T thermochronometers. b) Proposed source model for formation of the Questa porphyry Mo deposit. Scavenging of Mo occurs during a halogen-rich fluxing event during enriched mantle-derived mafic magma recharge into hybridized juvenile lower crust. Upper crustal reservoirs are minimal to absent, and the predicted T-t history crystallizes all zircon within uncertainty of low-T chronometers.

rarely on the relationship between ignimbrite generation and mineralization.

[47] Recent studies of volcanic-plutonic connections focus on magma flux variations responsible for ignimbrite and non-ignimbrite stages of volcanic field evolution [*Glazner et al*., 2004; *Lipman*, 2007; *Annen*, 2009; *Tappa et al*., 2011]. Although there are fundamental differences in interpretation among these papers, all agree that an unusually high flux of material (melt, fluid, gas) is required for formation of an ignimbrite as large as the Amalia Tuff (500 km^3). Most models also focus on the role of a high flux of material from the upper mantle to either remobilize an existing magma body [*Bachmann and Bergantz*, 2003; *Huber et al*., 2012] or initiate deep crustal melting [*Glazner et al*., 2004; *Tappa et al*., 2011].

[48] It is hypothesized here that the period of high magma flux responsible for generating the Amalia Tuff set the stage for generating mineralizing intrusions at Questa (Figure 8). A high flux of juvenile mafic rocks may have exsolved hydrothermal fluids during crystallization and created a zone of hybridized crust (juvenile mafic rocks + old lower crust + hydrothermal assemblages). *Stein* [1985] and *Stein and Hannah* [1985] analyzed sulfur isotopes from molybdenite and concluded that all of the sulfur in porphyry Mo systems is derived from the intrusions. Observing the same data, *Pettke et al*. [2010] emphasize that the ^{34}S values are consistent with a mantle source. Moreover, Pettke et al. [2010] used radiogenic Pb-isotopes to demonstrate that the mantle source was previously metasomatized, possibly during Proterozoic continental accretion. The high mafic magma flux required for formation of the ignimbrite rapidly transferred unusually high masses of material, including sulfur, into the lower crust as juvenile mafic rocks and hydrothermal fluids. Although mafic underplating throughout the history of the Latir field is hypothesized [*Johnson and Lipman*, 1988; *Johnson et al*., 1989, 1990] and thus, volatiles were presumably consistently transferred from the mantle to the crust, the unusually high flux necessary for

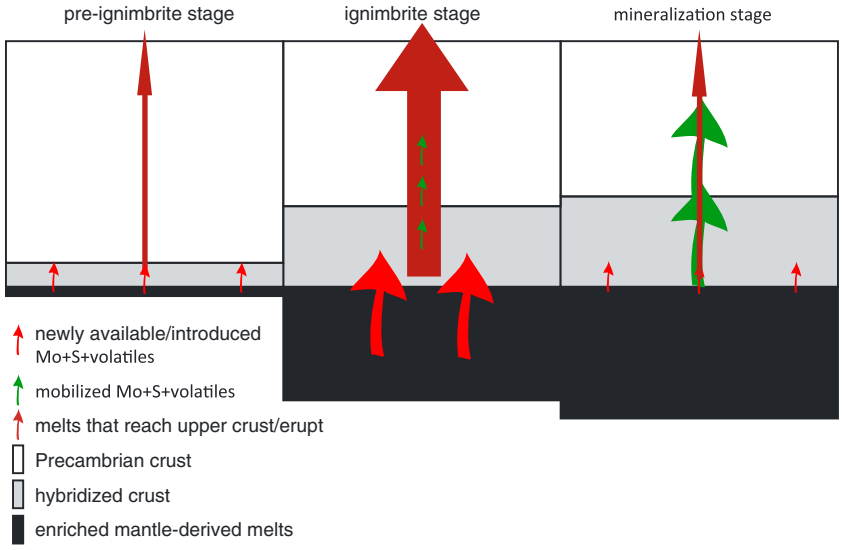

Figure 8. Schematic model showing the relationship between ignimbrite eruption and subsequent mineralization. Thickness of crust and juvenile mantle components are not drawn to scale. Relative size of arrows is proportional to input and output for respective fluxes. See text for discussion.

formation of the ignimbrite may have prepared the system for economic mineralization.

[49] Partial melting of the hybridized zone immediately following eruption of the Amalia Tuff produced granitic magmas capable of mineralization. Geochemical and experimental studies show that partial melting of hydrous amphibolites (~ lower crust) can create appreciable volumes of granitic magma [*Faure and Powell*, 1972; *Mahood and Halliday*, 1988; *Ratajeski et al.*, 2005]. Variable contributions from older lower crust, juvenile mafic rocks, and hydrothermal assemblages may explain slight compositional variations within productive intrusions at Questa (e.g., biotite-plagioclase porphyry [QM11-01] vs. quartz-alkali feldspar porphyry [QV11-02]). Metal endowment within the caldera margin plutons likely comes from a combination of (1) metal-rich lower crust source rocks and (2) release of volatiles during crystallization of underplating mafic magmas. These volatiles scavenge the metals and induce melting of the hybridized lower crust. According to this model, the halogen-rich volatilization that is typically inferred in porphyry Mo systems occurred during melting, rather than crystallization in an upper crustal magma reservoir [*Hildreth*, 1981; *Keith et al.*, 1986; *Carten et al.*, 1993; Figure 7b]. Moreover, this model can account for the observed components of both juvenile mafic rocks and much older (> 1 Ga) lower crust components within porphyry Mo magmas inferred from radiogenic isotope studies [*Farmer and DePaolo*, 1984; *Stein*, 1985; *Pettke et al.*, 2010].

[50] The proposed model for hybridized source rocks is similar to models proposed by *Richards* [2009, 2011]. However, our model emphasizes the relationship of porphyry Mo deposits to silicic ignimbrite systems, and not necessarily arc or back-arc tectonic regimes. Regardless, the post-ignimbrite mineralization observed in this study suggests that metasomatic preparation of the lower crust may be a critical step in generating productive intrusions.

[51] This model implies the general possibility that porphyry Mo mineralization follows ignimbrite eruption [e.g., *Lipman*, 2007]. The world's largest Climax-type deposits in Colorado are located close in space and time to the Eocene-Oligocene flare-up [*Chapin*, 2012] and the Pine Grove deposit in Utah immediately post-dates a small ignimbrite eruption that ended an ~4 Ma hiatus from the voluminous (~ 10,000 km^3) Indian Peak caldera complex [*Best et al.*, 1989; *Keith et al.*, 1986]. Drilling near the western rim of the ~1 Ma Valles caldera identified a shallow zone of molybdenum mineralization that is interpreted to be related to Climax-type mineralization at depth [*Hulen et al.*, 1987]. Climax-type mineralization has been inferred from elevated F contents in soils along the partial-ring intrusion of the Oligocene Bonanza caldera in Colorado as well [*Lipman*, 2007; *Rose and Pride*, 2010]. These observations argue strongly for a genetic relationship between caldera-forming eruptions and Mo mineralization wherein a major hybridization event provides unusually high masses of readily mobile metals and "prepares" the lower crust for

subsequent melting events that may produce productive magmas. Consequently, future exploration models should perhaps target caldera systems where post-ignimbrite intrusions can be identified. Additional detailed geothermochronology such as that presented here should be done to evaluate this hypothesis.

6. Conclusions

[52] New U/Pb zircon geochronology from the Latir volcanic field shows that mineralizing magmas were emplaced along the southern margin of the Questa caldera margin over 770 ka. Epithermal Au-Ag mineralization near the Red River intrusive complex, a possible source for mineral occurrences, post-dates caldera formation by at least 300 ka. Molybdenite Re/Os ages show that the Questa porphyry Mo deposit was assembled episodically over 250 ka between ~ 24.76 and 24.50 Ma, and the bulk of the mineralization was synchronous with the emplacement of suite of high-silica granites.

[53] This study demonstrates that Re/Os molybdenite geochronology can be used as a thermochronometer in cases where temperature can be determined independently. These data provide further evidence that the Re/Os chronometer remains closed to diffusion during repeated hydrothermal circulation events with temperatures in excess of ~400 °C. These data are used to show the complex thermal history of the incrementally assembled Questa porphyry Mo deposit.

[54] Detailed geo-thermochronology of the Questa Mo deposit is inconsistent with previous genetic models for the system that predict magma residence time in a long-lived system or simple evolution of mineralizing intrusions via fractional crystallization. The fact that Mo mineralization post-dates the eruption of the Amalia Tuff suggests a model wherein anomalously high magma flux mobilizes metals and sulfur from the mantle and lower crust. Scavenging and partial melting of the newly formed hybridized zone is hypothesized to create the magmas responsible for mineralization. This new model suggests that immediate post-ignimbrite plutons within calderas should be considered an important target for mineral exploration.

Acknowledgments

[55] We thank Amanda Rowe and Jean Cline for providing molybdenite samples from their personal collections. This project would not have been possible without the help of Bruce Walker and Chevron Mining Inc., who provided access to the mine property and advice throughout the project. Funding was provided by the National Science Foundation (EAR: 1050215), Geological Society of America, Sigma Xi Grants-in-Aid of Research, and the UNC Martin Fund. Thanks to Jez Inglis and Aaron Zimmerman for providing lab work and insight. Helpful reviews were provided by Eric Christiansen and an anonymous reviewer.

References

Annen, C. (2009), Implications of incremental emplacement of magma bodies for magma differentiation, thermal aureole dimensions and plutonism-volcanism relationships, *Tectonophysics*, doi:10.1016/j.tecto.2009.04.010.

Audétat, A. (2010), Source and evolution of molybdenum in the porphyry Mo [-Nb] deposit at Cave Peak, Texas, *J. Petrol.*, *51*, 1739–1760.

Bachmann, O., and G. W. Bergantz (2003), Rejuvenation of the Fish Canyon magma body: a window into the evolution of large-volume silicic magma systems, *Geology*, *31*, 789–792.

Becker, S. P., A. Fall, and R. J. Bodnar (2008), Synthetic fluid inclusions. XVII. PVTX properties of high salinity H_2O-NaCl solutions (> 30 wt % NaCl): Application to fluid inclusions that homogenize by halite disappearance from porphyry copper and other hydrothermal ore deposits, *Econ. Geol.*, *103*, 539–554.

Best, M. G., E. H. Christiansen, and R. H. Blank Jr. (1989), Oligocene caldera complex and calc-alkaline tuffs and lavas of the Indian Peak volcanic field, Nevada and Utah, *Geol. Soc. Am. Bull.*, *101*, 1076–1090.

Birck, J. L., M. R. Barman, and F. Capmas (1997), Re-Os isotopic measurements at the femtomole level in natural samples, *Geostand. Newslett.*, *20*, 19–27.

Bowring, J. F., N. M. McLean, and S. A. Bowring (2011), Engineering cyber infrastructure for U-Pb geochronology: Tripoli and U-Pb_Redux, *Geochem. Geophys. Geosyst.*, *12*, doi:10.1029/2010GC003479.

Braxton, D. P., D. R. Cooke, J. Dunlap, M. Norman, P. Reiners, H. Stein, and P. Waters (2012), From crucible to graben in 2.3 Ma: A high-resolution geochronological study of porphyry life cycles, Boyongan-Bayugo copper-gold deposits, Philippines, *Geology*, *40*(5), 471–474.

Burnham, C. W. (1997), Magmas and hydrothermal fluids, in Geochemistry of Hydrothermal Ore Deposits, edited by H. L. Barnes, 3rd ed., p. 63–123, John Wiley & Sons.

Candela, P. A. (1997), A review of shallow, ore-related granites: Textures, volatiles, and ore metals, *J. Petrol.*, *38*, 1619–1633.

Carten, R. B., E. P. Geraghty, B. M. Walker, and J. R. Shannon (1988a), Cyclic development of igneous features and their relationship to high-temperature hydrothermal features in the Henderson porphyry molybdenum deposit, Colorado, *Econ. Geol.*, *83*, 266–296.

Carten, R. B., B. M. Walker, E. P. Geraghty, and A. Gunow (1988b), Comparison of field-based studies of the Henderson porphyry molybdenum deposit, Colorado, with experimental and theoretical models of porphyry systems, in Canadian Institute of Mining and Metallurgy Special Volume 39, edited by Taylor, R. P., and D. F. Strong, 351–366.

Carten, R. B., W. H. White, and H. J. Stein (1993), High-grade granite-related molybdenum systems; classification and

origin, in Mineral deposit modeling: Geological Association of Canada Special Paper, 40, edited by R. V. Kirkham, W. D. Sinclair, R. I. Thorpe, and J. M. Duke, 521–544.

Cathles, L. M., A. H. J. Erendi, and T. Barrie (1997), How long can a hydrothermal system be sustained by a single intrusive event? *Econ. Geol.*, *92*, 766–771.

Chapin, C. E. (2012), Origin of the Colorado Mineral Belt, *Geosphere*, *8*, 28–43, doi:10.1130/GES00694.1

Cline, J. S., and R. J. Bodnar (1994), Direct evolution of a brine from a crystallizing silicic melt at Questa, New Mexico, molybdenum deposit, *Econ. Geol.*, *89*, 1780–1802.

Cohen, A. S., and F. G. Waters (1996), Separation of osmium from geological materials by solvent extraction for analysis by thermal ionization mass spectrometry, *Anal. Chim. Acta*, *332*, 269–275.

Coleman, D. S., W. Gray, and A. F. Glazner (2004), Rethinking the emplacement and evolution of zoned plutons: Geochronologic evidence for incremental assembly of the Tuolumne Intrusive Suite, California, *Geology*, *32*, 433–436.

Cordell, L., C. L. Long, and D. W. Jones (1985), Geophysical expression of the batholith beneath Questa caldera, New Mexico, *J. Geophys. Res.*, *90*, 11263–11269.

Davis, J. W., D. S. Coleman, J. T. Gracely, R. Gaschnig, and M. Stearns (2012), Magma accumulation rates and thermal histories of plutons of the Sierra Nevada batholith, CA, *Contrib. Mineral. Petr.*, *163*, 449–465, doi: 10.1007/s00410-011-0683-7

Farmer, G., and D. DePaolo (1984), Origin of Mesozoic and Tertiary granite in the western United States and implications for pre-Mesozoic crustal structure 2. Nd and Sr isotopic studies of unmineralized and Cu- and Mo-mineralized granite in the Precambrian Craton, *J. Geophys. Res.*, *89*, doi:10.1029/JB089iB12p10141.

Faure, G., and J. L. Powell (1972), Strontium isotope geology, Springer, Berlin Heidelberg, New York.

Fournier, R. O. (1999), Hydrothermal processes related to movement of fluid from plastic into brittle rock in the magmatic-epithermal environment, *Econ. Geol.*, *94*, 1193–1211.

Glazner, A. F., J. M. Bartley, D. S. Coleman, W. Gray, and R. Z. Taylor (2004), Are plutons assembled over millions of years by amalgamation from small magma chambers? *GSA Today*, *14*, 4–11.

Hanson, R. B., and A. F. Glazner (1995), Thermal requirements for extensional emplacement of granitoids, *Geology*, *23*, 213–216.

Harrison, T. M. (1981), Diffusion of ^{40}Ar in hornblende, *Contrib. Mineral. Petr.*, *78*, 324–331.

Harrison, T. M., I. Duncan, and I. McDougall (1985), Diffusion of ^{40}Ar in biotite: Temperature, pressure and compositional effects, *Geochim. Cosmochim. Acta*, *49*, 2461–2468.

Henry, C. D., H. B. Elson, W. C. McIntosh, M. T. Heizler, and S. B. Castor (1997), Brief duration of hydrothermal activity at Round Mountain, Nevada, determined from ^{40}Ar/^{39}Ar geochronology, *Econ. Geol.*, *92*, 807–826.

Hildreth, W. (1981), Gradients in silicic magma chambers: Implications for lithospheric magmatism, *J. Geophys. Res.*, *86*, 10153–10192.

Huber C., O. Bachmann, and J. Dufek (2012), Crystal-poor verses crystal-rich ignimbrites: A competition between stirring and reactivation, *Geology*, *40*, 115–118.

Hulen J. B., D. L. Nielson, F. Goff, J. N. Gardner, and R. W. Charles (1987), Molybdenum mineralization in an active geothermal system, Valles caldera, New Mexico, *Geology*, *15*, 748–752.

Jaffey, A. H., K. F. Flynn, L. E. Glendenin, W. C. Bently, and A. M. Essling (1971), Precision measurement of the half-lives and specific activities of U235 and U238, *Phys. Rev. C*, *4*, 1889–1906.

Johnson, C. M., and P. W. Lipman (1988), Origin of metaluminous and alkaline volcanic rocks of the Latir volcanic field, northern Rio Grande rift, New Mexico, *Contrib. Mineral. Petr.*, *100*, 107–128.

Johnson, C. M., G. K. Czamanske, and P. W. Lipman (1989), Geochemistry of intrusive rocks associated with the Latir volcanic field, New Mexico, and contrasts between evolution of plutonic and volcanic rocks, *Contrib. Mineral. Petr.*, *103*, 90–109.

Johnson, C. M., P. W. Lipman, and G. K. Czamanske (1990), H, O, Sr, Nd, and Pb isotope geochemistry of the Latir volcanic field and cogenetic intrusions, New Mexico, and relations between evolution of a continental magmatic center and modifications of the lithosphere, *Contrib. Mineral. Petr.*, *104*, 99–124.

Keith, J. D., W. C. Shanks, D. A. Archibald, and E. Farrar (1986), Volcanic and intrusive history of the Pine Grove porphyry molybdenum system, southwestern Utah, *Econ. Geol.*, *81*, 553–577.

Klemm, L. M., T. Pettke, and C. A. Heinrich (2008), Fluid and source magma evolution of the Questa porphyry Mo deposit, New Mexico, USA, *Miner. Deposita*, *43*, 533–552.

Lawley, C. J. M., J. P. Richards, R. G. Anderson, R. A. Creaser, and L. M. Heaman (2010), Geochronology and geochemistry of the MAX porphyry Mo deposit and its relationship to Pb-Zn-Ag mineralization, Kootenay arc, southeastern British Columbia, Canada, *Econ. Geol.*, *105*, 1113–1142.

Leuthold, J., O. Müntener, L. P. Baumgartner, B. Putlitz, M. Ovtcharova, and U. Schaltegger (2012), Time resolved construction of a bimodal laccolith [Torres del Paine, Patagonia], *Earth Planet. Sci. Lett.*, *325*, 85–92.

Lipman, P. W. (1988), Evolution of silicic magma in the upper crust: The mid-Tertiary Latir volcanic field and its cogenetic granitic batholith, northern New Mexico, U.S.A., *Trans. R. Soc. Edinburgh: Earth Sci.*, *79*, 265–288.

Lipman, P. W. (1992), Ash-flow calderas as structural controls of ore deposits — recent work and future problems, *U. S. Geol. Surv. Bull.*, *2012*, L1–L12.

Lipman, P. W. (2006), Geologic map of the central San Juan caldera cluster, southwestern Colorado, *Pamphlet to accompany U.S. Geol. Surv. Map*, *I-2799*, 37 p.

Lipman, P. W. (2007), Incremental assembly and prolonged consolidation of Cordilleran magma chambers; evidence from the Southern Rocky Mountain volcanic field, *Geosphere*, *3*, 42–70.

Lipman, P. W., H. H. Mehnert, and C. M. Naeser (1986), Evolution of the Latir volcanic field, northern New Mexico, and its relation to the Rio Grande rift, as indicated by potassium-argon and fission track dating, *J. Geophys. Res.*, *91*, 6329–6345.

Lipman, P. W., and J. C. Reed (1989), Geologic map of the Latir volcanic field and adjacent areas, northern New Mexico, *U.S. Geol. Surv. Map*, *I-1907*, *scale 1:48,000*.

Lowell, J. D., and J. M. Guilbert (1970), Lateral and vertical alteration-mineralization zoning in porphyry ore deposits, *Econ. Geol.*, *65*, 373–408.

Lowenstern, J. (1994), Dissolved volatile concentrations in an ore-forming magma, *Geology*, *22*, 893–896.

Mahood G. A., and A. N. Halliday (1988), Generation of high-silica rhyolite; a Nd, Sr, and O isotopic study of Sierra La Primavera, Mexican neovolcanic belt, *Contrib. Mineral. Petr.*, *100*, 183–191.

Maksaev, V., F. Munizaga, M. McWilliams, M. Fanning, R. Mathur, J. Ruiz, and M. Zentilli (2004), New chronology for El Teniente, Chilean Andes, from U-Pb, ^{40}Ar/^{39}Ar, Re-

Os and fission-track dating: Implications for the evolution of a supergiant porphyry Cu-Mo deposit, *Soc. Econ. Geol. Special Publication*, *11*, 15–54.

Markey, R., J. L. Hannah, J. W. Morgan, and H. J. Stein (2003), A double spike for osmium analysis of highly radiogenic samples, *Chem. Geol.*, *200*, 395–406.

Marsh, T. M., T. M. Einaudi, and M. McWilliams (1997), $^{40}Ar/^{39}Ar$ geochronology of Cu-Au and Au-Ag mineralization in the Potrerillos district, Chile, *Econ. Geol.*, *92*, 784–806.

Mattinson, J. M. (2005), Zircon U-Pb chemical abrasion [CA-TIMS] method: Combined annealing and multi-step dissolution analysis for improved precision and accuracy of zircon ages, *Chem. Geol.*, *220*, 47–56.

Matzel, J. E. P., S. A. Bowring, and R. B. Miller (2006), Time scales of pluton construction at differing crustal levels; examples from the Mount Stuart and Tenpeak intrusions, north Cascades, Washington, *Geol. Soc. Am. Bull.*, *118*(11-12), 1412–1430.

McLean, N. M., J. F. Bowring, and S. A. Bowring (2011), An algorithm for U-Pb isotope dilution data reduction and uncertainty propagation, *Geochem. Geophys. Geosys.*, *12*, doi:10.1029/2010GC003478.

McLemore, V. T., and R. M. North (1984), Occurrences of precious metals and uranium along the Rio Grande rift in northern New Mexico, *New Mexico Geol. Society Guidebook*, *35th Field Conference.*

Meyer, J. (1991), Volcanic, plutonic, tectonic, and hydrothermal history of the southern Questa caldera, New Mexico, Ph.D thesis, University of California at Santa Barbara, Santa Barbara.

Meyer, J., and K. A. Foland (1991), Magmatic-tectonic interaction during early Rio Grande Rift extension at Questa, New Mexico, *Geol. Soc. Am. Bull.*, *103*, 993–1006.

Pettke, T., F. Oberli, and C. A. Heinrich (2010), The magma and metal source of giant porphyry-type ore deposits, based on lead isotope microanalysis of individual fluid inclusions, *Earth Planet. Sci. Lett.*, *296*, 267–277, doi:10.1016/j.epsi.2010.05.007.

Ratajeski, K., T. W. Sisson, and A. F. Glazner (2005), Experimental and geochemical evidence for derivation of the El Capitan Granite, California, by partial melting of hydrous gabbroic lower crust, *Contrib. Mineral. Petr.*, *149*, 713–734.

Richards, J. P. (2009), Postsubduction porphyry Cu-Au and epithermal Au deposits: Products of remelting of subduction-modified lithosphere, *Geology*, *37*(3), 247–250.

Richards, J. P. (2011), Magmatic to hydrothermal metal fluxes in convergent and collided margins, *Ore Geol. Rev.*, *40*, 1–26.

Rose, M., and D. E. Pride (2010), "Target mapping" at Bonanza, Colorado: Integrating geology, geochemistry, and mineralization models in a caldera setting, *Abstracts with Programs – Geological Society of America*, *42*, 54.

Ross, P. S., M. Jèbrak, and B. M. Walker (2002), Discharge of hydrothermal fluids from a magma chamber and concomitant formation of a stratified breccia zone at the Questa porphyry molybdenum deposit, New Mexico, *Econ. Geol.*, *97*, 1679–1699.

Rowe, A. (2012), Fluid evolution of the magmatic-hydrothermal breccia of the Goat Hill ore body, Questa Climax-type porphyry molybdenum system, New Mexico — a fluid inclusion study, Ph.D thesis, New Mexico Institute of Mining and Technology, Socorro.

Rytuba, J. J. (1994), Evolution of volcanic and tectonic features in caldera settings and the importance in the localization of ore deposits, *Econ. Geol.*, *89*, 1687–1696.

Seedorff, E., and M. T. Einaudi, (2004a), Henderson porphyry molybdenum system, Colorado: I. Sequence and abundance of hydrothermal mineral assemblages, flow paths of evolving fluids, and evolutionary style, *Econ. Geol.*, *99*, 3–37.

Seedorff, E., and M. T. Einaudi (2004b), Henderson porphyry molybdenum system, Colorado: II. Decoupling of introduction and deposition of metals during geochemical evolution of hydrothermal fluids, *Econ. Geol.*, *99*, 37–70.

Selby, D., B. E. Nesbitt, K. Muehlenbachs, and W. Prochaska (2000), Hydrothermal alteration and fluid chemistry of the Endako porphyry molybdenum deposit, British Columbia, *Econ. Geol.*, *95*, 183–202.

Selby, D., R. A. Creaser, H. J. Stein, R. J. Markey, and J. L. Hannah (2007), Assessment of the ^{187}Re decay constant by cross calibration of Re-Os molybdenite and U-Pb zircon chronometers in magmatic ore systems, *Geochim. Cosmochim. Acta*, *71*(8), 1999–2013.

Shirey, S. B., and R. J. Walker (1995), Carius tube digestion for low-blank rhenium-osmium analysis, *Anal. Chem.*, *67*, 2136–2141.

Singer, B., and P. Marchev (2000), Temporal evolution of arc magmatism and hydrothermal activity including epithermal gold veins, Borovitsa caldera, southern Bulgaria, *Econ. Geol.*, *95*, 1155–1164.

Smoliar, M. I., R. J. Walker, and J. W. Morgan (1996), Re/Os ages of group IIA, IIIA, IVA, and IVB iron meteorites, *Science*, *271*, 1099–1102.

Spera, F. (1980), Thermal evolution of plutons: A parameterized approach, *Science*, *207*, 299–301.

SRK Consulting (U.S.), Inc. (2004), Molycorp Questa — Report on geologic mapping and cross section project, *Unpublished report for Molycorp*, *Inc.*, 82 p.

Stacey, J. S., and J. D. Kramers (1975), Approximation of terrestrial lead isotope evolution by a two-stage model, *Earth Planet. Sci. Lett.*, *26*, 207–221.

Stein, H. J. (1985), A Lead, Strontium, and Sulfur Isotope Study of Laramide-Tertiary Intrusions and Mineralization in the Colorado Mineral Belt with Emphasis on Climax-type Porphyry Molybdenum Systems plus a Summary of Other Newly Acquired Isotopic and Rare Earth Element Data, University of North Carolina at Chapel Hill, PhD dissertation, 493 p.

Stein, H. J. (2006), Low-rhenium molybdenite by metamorphism in northern Sweden: Recognition, genesis, and global implications, *Lithos*, *87*, 300–327.

Stein, H. J., and J. L. Hannah (1985), Movement and origin of ore fluids in Climax-type systems, *Geology*, *13*, 469–474.

Stein, H. J., J. W. Morgan, R. J. Markey, A. E. Williams-Jones, M. Heiligmann, and J. R. Clark (1999), Re-Os age for the Hemlo Au deposit, Ontario, Canada: Durability of the Re-Os chronometer, *EOS Trans. AGU*, *80*, F1082.

Stein, H. J., R. J. Markey, J. W. Morgan, J. L. Hannah, and A. Scherstén (2001), The remarkable Re-Os chronometer in molybdenite: How and why it works, *Terra Nova*, *13*, 479–486.

Stein, H. J., and B. Bingen (2002), 1.05-1.01 Ga Sveconorwegian metamorphism and deformation of the supracrustal sequence at Sæsvatn, south Norway: Re-Os dating of Cu-Mo mineral occurrences, in D. Blundell, F. Neubauer, and A. von Quadt, (eds.), The Timing and Location of Major Ore Deposits in an Evolving Orogen, *Geological Society*, *London*, *Special Publications*, *204*, 319–335.

Stein, H. J., A. Scherstén, J. Hannah, and R. Markey (2003), Subgrain-scale decoupling of Re and ^{187}Os and assessment of laser ablation ICP-MS spot dating in molybdenite, *Geochim. Cosmochim. Acta*, *67*, 3673–3686, doi:10.1016/S0016-7037[00]00269-2.

Suzuki, K., Shimizu, H., and A. Masuda (1996), Re-Os dating of molybdenites from ore deposits in Japan: Implication for the closure temperature of the Re-Os system for molybdenite and the cooling history of molybdenum ore deposits, *Geochim. Cosmochim. Acta*, *60*, 3151–3159.

Tappa, M. J., D. S. Coleman, R. D. Mills, and K. M. Samperton (2011), The plutonic record of a silicic ignimbrite from the Latir volcanic field, New Mexico, *Geochem. Geophys. Geosys.*, *12*, Q10011, doi:10.1029/2011GC003700

U.S. Geological Survey (2011), Molybdenum, Mineral Commodity Summaries.

von Quadt, A., M. Erni, K. Martinek, M. Moll, I. Peytcheva, and C. Heinrich (2011), Zircon crystallization and the lifetimes of ore-forming magmatic-hydrothermal systems, *Geology*, *39*, 731–734.

Wallace, S. R., N. K. Muncaster, D. C. Jonson, W. B. MacKenzie, A. A. Bookstrom, and V. E. Surface (1968), Multiple intrusion and mineralization at Climax, Colorado, in Ore deposits of the United States, 1933–1967: New York, American Institute Mining Metallurgy and Petroleum Engineers, 1, edited by J. D. Ridge, 605–640.

Watson, E. B., and T. M. Harrison (1983), Zircon saturation revisited: Temperature and composition effects in a variety of crustal magma types, *Earth Planet. Sci. Lett.*, *64*, 295–304.

White, W. H., A. A. Bookstrom, R. J. Kamilli, M. W. Ganster, R. P. Smith, D. E. Ranta, and R. C. Steininger (1981), Character and origin of Climax-type molybdenum deposits, *Econ. Geol. 75th Anniversary Volume*, 270–316.

Wilson, A. J., D. R. Cooke, H. J. Stein, M. C. Fanning, J. R. Holliday, and I. J. Tedder (2007), U-Pb and Re-Os geochronologic evidence for two alkali porphyry ore-forming events in the Cadia district, New South Wales, Australia, *Econ. Geol.*, *102*, 3–26.

Yoshinobu, A. S., D. A. Okaya, and S. R. Paterson (1998), Modeling the thermal evolution of fault-controlled magma emplacement models: Implications for the solidification of granitoid plutons, *J. Struct. Geol.*, *20*, 1205–1218.

Zimmerer, M. J., and W. C. McIntosh (2012), The Ar/Ar geo- and thermochronology of the Latir volcanic field and the associated intrusions: Understanding caldera magmatic processes using the volcanic-plutonic relationship, *Geol. Soc. Am. Bull.*, doi:10.1130/B30544.1

Zimmerman, A., H. J. Stein, J. L. Hannah, D. Koželj, K. Bogdanov, and T. Berza (2008), Tectonic configuration of the Aspuseni-Banat-Timok-Srednogorie belt, Balkans-South Carpathians, constrained by high precision Re/Os molybdenite ages, *Miner. Deposit*, *43*, 1–21.